Supplementary Figures and Methods

Top-down laminar organization of the excitatory network in motor cortex

Nicholas Weiler, Lydia Wood, Jianing Yu, Sara A. Solla, & Gordon M. G. Shepherd

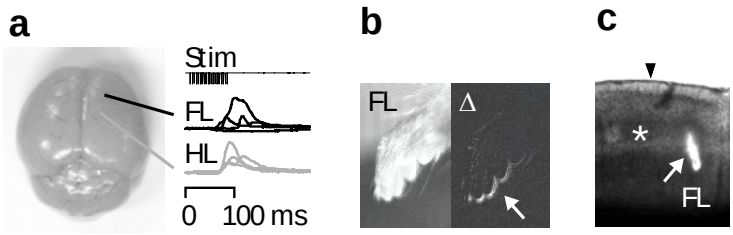

Supplementary Fig. 1. Identification of the M1 *in vitro* mapping territory as a forelimb-related somatic representation zone. (A) Trains of <50 μA ICMS stimulus pulses at the indicated M1 locations generated forelimb (FL) or hindlimb (HL) movements, as monitored by photodiode. (B) Movement of the forepaw in response to ICMS in the FL region, monitored by video (left) and illustrated by subtracting frames acquired immediately before and after the stimulus (Δ, right). (C) Fluorescent beads injected *in vivo* into ICMS sites in the FL region were subsequently identified in M1 slices anterior to the M1/S1 border (▼); an S1 barrel is marked (*).

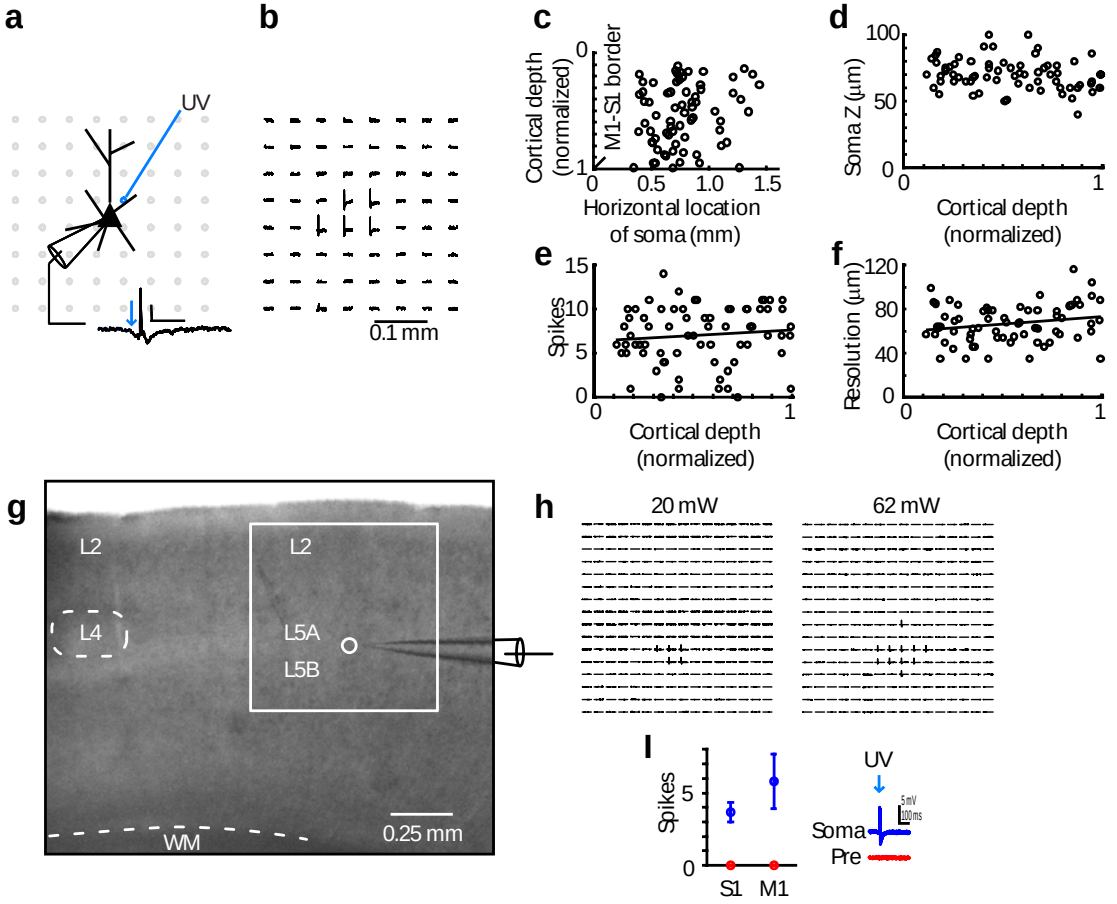

Supplementary Fig. 2. Calibration of LSPS in M1 with excitation profiles. (A) Schematic of loose-seal recording of spikes during photostimulation. Array of circles represents stimulus grid. (B) Array of traces in typical excitation profile of M1 L2/3 neuron. Spikes were evoked by stimulation in the perisomatic region. Spacing between rows and columns was 50 µm. (C) Excitation profiles were recorded from cells distributed across the horizontal and vertical expanse of M1 in the slice. Cortical depth refers to normalized soma location along the vertical axis, with pia = 0 and white matter = 1. (D) The somata of the recorded neurons were at comparable depths across layers. (E) Number of spikes per cell evoked by photostimulation was layer independent. (F) The resolution of photostimulation was ~70 µm across layers. (G) Recording arrangement in experiments designed to assess feedforward driving. In this example, a neuron in L5A/B in M1 was recorded in loose-seal mode while stimulating L2 and other locations providing strong excitatory input. (H) Excitation profiles from the experiment in G, showing only perisomatic, not feedforward, excitation, even at much higher stimulus intensities. (I) Summary data from 8 neurons in M1 and S1 tested for feedforward excitation as above. Blue, data for perisomatic stimuli; red, data for presynaptic stimuli. Error bars: s.e.m.

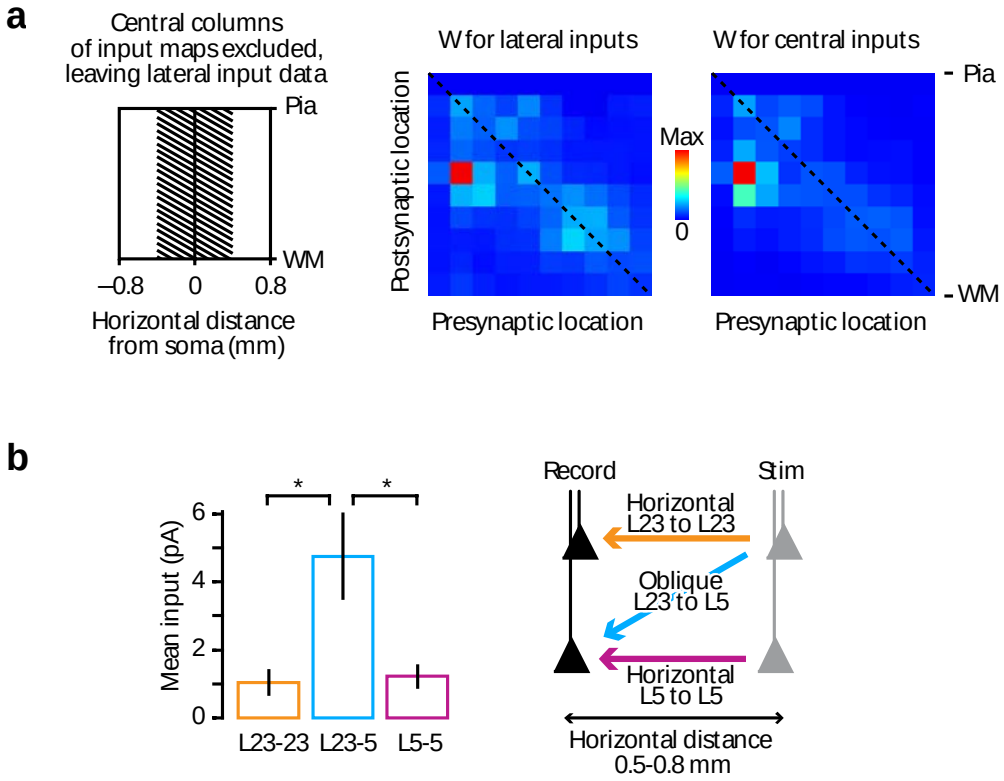

Supplementary Fig. 3. Analysis of laterally offset inputs. (A) The central half (middle 8 data columns) of the recorded input maps were excluded, leaving data points from stimuli located >0.4 mm lateral to the soma. The connectivity matrix calculated with this subset of the data (left image) closely resembles that obtained with the full data set (cf. Fig. 1f) and that obtained using only the central half of the maps (right image). Data were normalized to the peak value in each matrix to facilitate comparison. (B) Maps of L2/3 neurons (n = 16 neurons) were pooled, averaged, and analyzed to calculate the strength of horizontal inputs arising from locations in L2/3 that were >0.5 mm lateral to the soma (orange). The same analysis was performed for L5 neurons (n = 16), but for horizontal inputs arising from lateral locations in L5 (magenta) and oblique inputs arising from lateral locations in L2/3 (blue). Oblique L2/3→5 inputs were stronger than horizontal L2/3→2/3 and L5→5 inputs despite the longer path distance, which would be expected to render oblique axons more vulnerable to slicing (*: $p < 0.05$, t-tests; n = 16–17 cells per group). Error bars: s.e.m.

Supplementary Methods

Intracortical microstimulation (ICMS). We used standard methods for ICMS in mice [1]. Animals were anesthetized with ketamine/xylazine and mounted in a stereotaxic frame (Kopf), and a dorsal craniotomy over the right hemisphere was opened to expose M1 for ICMS. Stimulating currents (20–50 μA) were delivered by glass electrodes, ~20 μm tip diameter. Motor responses were recorded either by photodiode (Edmund Optics) to detect temporal aspects of movement (Supplementary Fig. 1A), or by CCD camera to detect spatial aspects of movement (Supplementary Fig. 1B). For the former, the beam path of a red laser (635 nm; ~1 mW) was partially obscured from striking the photodiode by the animal's dangling forelimb or hindlimb, enabling small movements to be transduced as changes in the photodiode current, and thus providing a measure of the time course of the movements. These currents were filtered, amplified, and sampled at 10 KHz. In 5 animals, sites generating forelimb movements were located at stereotaxic coordinates 0–0.5 mm rostrocaudal and 1.5–2.0 mm lateral [1, 2]. In 2 animals, red fluorescent beads (Lumafluor) were pressure-injected (Picospritzer III, General Valve) at a stimulation site generating forelimb movements, and subsequent recovered in the M1 region of slices; labeling was found in the territory in which neurons were recorded in LSPS mapping experiments (Supplementary Fig. 1C).

Calibration of LSPS using excitation profiles. We quantitatively estimated the photoexcitability of M1 pyramidal neurons using excitation profiles (Supplementary Fig. A,B), which are loose-seal recordings of LSPS-evoked spikes from neurons located in the presynaptic fields of interest [3-5]; similar approaches have been used by others [6, 7]. Because

neurons throughout M1 were within the mapping region-of-interest, we recorded excitation profiles from neurons located in all layers (Supplementary Fig. 2C), and at the same approximate depth in the slice, ~0.05-0.1 mm (Supplementary Fig. 2D). The standard grid was an 8–by–8 array centered on the soma, with 0.05 mm spacing; the pixel area (A_{pixel}) was 0.0025 mm^2. In addition, we routinely also acquired larger excitation profiles (by increasing grid spacing or array size) to ensure that the zone of excitable sites was fully covered. From the excitation profile data set (n = 70 pyramidal neurons, distributed approximately evenly across layers) we estimated the number of spikes per excitation profile (S_{neuron}) as 7.0 ± 3.3 spikes $cell^{-1}$ (mean ± s.d.), the number of spikes per (non-zero) pixel (S_{pixel}) as 1.1 ± 0.1 spikes $cell^{-1}$ (mean ± s.d.), and the resolution (R; distance from soma of spike-evoking pixels, weighted by the number of spikes) as 0.067 ± 0.017 mm (mean ± s.d.) (Supplementary Fig. 2E,F). Neuronal density (ρ) in mouse motor/frontal cortex [8-10] is ~10^5 neurons mm^{-3}. From

(Eqn. 1) $$N_{spiking} = \rho A_{pixel} R S_{neuron} / S_{pixel}$$

we estimated $N_{spiking} \approx 100$ spiking neurons per stimulus. We emphasize both that this is only a rough estimate, and that the exact value is not critical for interpretation of the connectivity matrix, which indicates the *relative* strengths of pathways connecting small clusters of neurons at different locations along the radial axis of the cortex.

Although LSPS maps can be normalized for layer-specific photoexcitability parameters [11], this was unnecessary as we did not observe such differences in M1 (Supplementary Fig. 2E,F). We also did not attempt to normalize for possible laminar variations in ρ in mouse M1, which however is unlikely to vary by more than a factor of ~2 (based on mouse S1 measurements [12, 13]).

We performed additional control experiments to assess for synaptic driving (feedforward excitation) in these slices. Synaptic driving would appear in excitation profiles as spike-evoking sites away from the perisomatic area of the neuron. In previous experiments in barrel cortex both in rats [4] and mice [14], conditions were found that strongly reduced excitability, including the presence of high divalents in the bath solution and blockade of NMDA receptor currents, and because similar excitability-reducing conditions were used here we expected driving to be minimal or undetectable. Driving would most likely occur in the strongest excitatory pathways. Therefore we recorded from the 'downstream' neurons – L5 neurons in M1, and L2/3 neurons in adjacent S1 – in the strongest excitatory pathways identified in these slices – L2/3→5 in M1, and L4→2/3 in S1. Stimulating the presynaptic neurons in these strong excitatory pathways did not evoke spikes in the postsynaptic neuron (0/8 cells) (Supplementary Fig. 2G-I). Thus, in this direct test we did not find evidence of synaptically driven spiking evoked by photostimulation. Additional evidence against synaptically driven spiking comes from power series mapping experiments (data not shown), in which synaptic input maps were acquired using a wide range of stimulus intensities. Synaptic driving should appear in synaptic input maps as a loss of detail causing 'smearing' of map structure; however, even at nearly double the standard mapping intensity the topography of maps was unchanged; i.e., varying the intensity simply scaled the 'brightness' of the maps. From these control and calibration experiments we conclude that synaptic inputs mapped in LSPS experiments are maps of monosynaptic input.

Reversal potential for GABAergic conductances. We used UV laser photolysis of caged GABA to determine the reversal potential for GABAergic inhibitory conductances. Caged GABA (100 μM; Invitrogen) was added to the bath solution along with tetrodotoxin (1 μM; Tocris), and neurons were recorded over a range of holding potentials while uncaging GABA at targeted somatodendritic locations with UV flashes at 20 mW. For three neurons (2 layer 5 pyramidal neurons and 1 layer 2/3 pyramidal neuron) we determined the mean response to GABA stimulation over the same time window used to analyze synaptic responses in synaptic input maps, and then calculated reversal potentials based on the measured current-voltage relationships. The average GABAergic reversal potential was –70.4 ± 1.8 mV (mean ± s.d.).

General comments on interpreting LSPS data.

For discussion of general advantages and limitations of LSPS as well as a variety of factors that are important to take into consideration in interpreting LSPS data the reader is referred to [3-5, 15]. Here, we highlight issues particularly relevant to the present study.

(i) Due to slicing, very long distance and/or very circuitous connections are prone to be underestimated in the spatial survey of inputs with LSPS. However, we observed robust connectivity on the scale of the local mapping territory used here (within ~1.5 mm of the soma). Furthermore, similar results were obtained when the central columns of the input maps were excluded from the analysis (Supplementary Fig. 3), indicating that the strong descending pathways were not due to radial pathways that might be preferentially preserved in the slice preparation. It is important to note that although LSPS maps will be

weighted towards more local connections, most intracortical connections are very local, including those within M1 [16-20].

(ii) Very local connections (~<100 from the soma) are likely to be underestimated, as traces that are contaminated by direct somatodendritic responses are rejected.

(iii) The analyses performed here involve averaging at multiple levels, from currents to pixels to maps. Thus, this approach is sensitive for identifying common (stereotypic) circuit patterns, but rarer ones may be averaged away.

(iv) Because disinhibition causes epileptiform discharges in neocortical slices (see below), we did not block inhibitory circuits. Instead, we isolated excitatory currents by recording at –70 mV, which was the experimentally measured reversal potential for GABAergic conductances as determined in separate experiments by GABA uncaging (see above). Through shunting inhibition, inhibitory inputs could in principle have reduced the magnitude of excitatory inputs. However, in general we believe this would have been at most a minor effect, because previous photostimulation experiments have shown most inhibitory inputs to excitatory neurons to arise from local intralaminar sites, not interlaminar locations [4, 6]; see also [21].

(v) The data provide only a 'somatocentric' view of the excitatory circuits we mapped, because we only recorded from neuronal somata, not dendrites. Pathways providing electrotonically remote inputs could have been underestimated.

Supplementary References

1. Li, C. X. & Waters, R. S. Organization of the mouse motor cortex studied by retrograde tracing and intracortical microstimulation (ICMS) mapping. Can J Neurol Sci 18, 28-38 (1991).
2. Paxinos, G. & Franklin, K. B. J. The mouse brain in stereotaxic coordinates (Academic Press, London, 2001).

3. Shepherd, G. M. G. in Visualizing Large-Scale Patterns of Activity in the Brain: Optical and Electrical Signals (ed. Buzsáki, G.) (Society for Neuroscience, Washington, D.C., 2006).

4. Shepherd, G. M. G., Pologruto, T. A. & Svoboda, K. Circuit analysis of experience-dependent plasticity in the developing rat barrel cortex. Neuron 38, 277-89. (2003).

5. Shepherd, G. M. G. & Svoboda, K. Laminar and columnar organization of ascending excitatory projections to layer 2/3 pyramidal neurons in rat barrel cortex. J. Neurosci. 25, 5670 (2005).

6. Dantzker, J. L. & Callaway, E. M. Laminar sources of synaptic input to cortical inhibitory interneurons and pyramidal neurons. Nat Neurosci 3, 701-7 (2000).

7. Schubert, D. et al. Layer-specific intracolumnar and transcolumnar functional connectivity of layer V pyramidal cells in rat barrel cortex. J Neurosci 21, 3580-92. (2001).

8. Cragg, B. G. The density of synapses and neurones in the motor and visual areas of the cerebral cortex. J Anat 101, 639-54 (1967).

9. Schuz, A. & Palm, G. Density of neurons and synapses in the cerebral cortex of the mouse. J Comp Neurol 286, 442-55 (1989).

10. Turnley, A. M., Faux, C. H., Rietze, R. L., Coonan, J. R. & Bartlett, P. F. Suppressor of cytokine signaling 2 regulates neuronal differentiation by inhibiting growth hormone signaling. Nat Neurosci 5, 1155-62 (2002).

11. Bureau, I., Shepherd, G. M. & Svoboda, K. Precise development of functional and anatomical columns in the neocortex. Neuron 42, 789-801 (2004).

12. Ransome, M. I., Goldshmit, Y., Bartlett, P. F., Waters, M. J. & Turnley, A. M. Comparative analysis of CNS populations in knockout mice with altered growth hormone responsiveness. Eur J Neurosci 19, 2069-79 (2004).

13. Ransome, M. I. & Turnley, A. M. Analysis of neuronal subpopulations in mice over-expressing suppressor of cytokine signaling-2. Neuroscience 132, 673-87 (2005).

14. Bureau, I., von Saint Paul, F. & Svoboda, K. Interdigitated Paralemniscal and Lemniscal Pathways in the Mouse Barrel Cortex. PLoS Biol 4, e382 (2006).

15. Shepherd, G. M. G., Stepanyants, A., Bureau, I., Chklovskii, D. B. & Svoboda, K. Geometric and functional organization of cortical circuits. Nature Neuroscience 8, 782-790 (2005).

16. Asanuma, H. & Rosen, I. Spread of mono- and polysynaptic connections within cat's motor cortex. Exp Brain Res 16, 507-20 (1973).

17. Landry, P., Labelle, A. & Deschenes, M. Intracortical distribution of axonal collaterals of pyramidal tract cells in the cat motor cortex. Brain Res 191, 327-36 (1980).

18. Keller, A. Intrinsic synaptic organization of the motor cortex. Cereb Cortex 3, 430-41 (1993).

19. Matsumura, M., Chen, D., Sawaguchi, T., Kubota, K. & Fetz, E. E. Synaptic interactions between primate precentral cortex neurons revealed by spike-triggered averaging of intracellular membrane potentials in vivo. J Neurosci 16, 7757-67 (1996).

20. Schieber, M. H. Constraints on somatotopic organization in the primary motor cortex. J Neurophysiol 86, 2125-43 (2001).

21. Binzegger, T., Douglas, R. J. & Martin, K. A. A quantitative map of the circuit of cat primary visual cortex. J Neurosci 24, 8441-53 (2004).